considerable changes in the framework geometry as confirmed by in situ single-crystal and powder x-ray diffraction measurements. The material is distinct in having a nanoporous host lattice chemistry (pore size, shape, and electronic potential) that may be manipulated in a switchable fashion, in this case by the external stimulation of spin crossover by temperature variation. Conversely, the reversible exchange of guest species has been shown to provide a unique mechanism with which to conveniently perturb the geometry and electronic environment of spin crossover centers, introducing a previously unstudied approach for the systematic investigation of this phenomenon. We note here that the desorption and resorption of guest species promises to provide an additional stimulus for spin crossover, suggesting potential application in areas such as molecular sensing (change in the color, magnetism, size, shape, etc. of the host with guest sorption). In the longer term, it is anticipated that the inclusion of guest and template species with specific electronic functions into molecular lattices that have controllable switching, including communication between these switching centers through coordination linkages, may lead to more advanced materials having other unique and potentially useful physicochemical properties.

References and Notes

1. M. D. Hollingsworth, *Science* **295**, 2410 (2002).
2. J. M. Lehn, *Science* **295**, 2400 (2002).
3. B. F. Hoskins, R. Robson, *J. Am. Chem. Soc.* **112**, 1546 (1990).
4. M. Eddaoudi *et al.*, *Science* **295**, 469 (2002).
5. C. J. Kepert, T. J. Prior, M. J. Rosseinsky, *J. Am. Chem. Soc.* **122**, 5158 (2000).
6. J. S. Seo *et al.*, *Nature* **404**, 982 (2000).
7. M. J. Zaworotko, *Nature* **402**, 242 (1999).
8. A. V. Nossov, D. V. Soldatov, J. A. Ripmeester, *J. Am. Chem. Soc.* **123**, 3563 (2001).
9. P. Gütlich, Y. Garcia, H. A. Goodwin, *Chem. Soc. Rev.* **29**, 419 (2000).
10. S. Decurtins, P. Gütlich, C. P. Köhler, H. Spiering, A. Hauser, *Chem. Phys. Lett.* **105**, 1 (1984).
11. O. Kahn, C. J. Martinez, *Science* **279**, 44 (1998).
12. E. Breuning *et al.*, *Angew. Chem. Int. Ed.* **39**, 2504 (2000).
13. S. Brooker, P. G. Plieger, B. Moubaraki, K. S. Murray, *Angew. Chem. Int. Ed.* **38**, 408 (1999).
14. J. A. Real *et al.*, *Science* **268**, 265 (1995).
15. N. Moliner *et al.*, *Inorg. Chem.* **39**, 5390 (2000).
16. Y. Garcia *et al.*, *Inorg. Chem.* **38**, 4663 (1999).
17. A. Ozarowski, Y. Shunzhong, B. R. McGarvey, A. Mislankar, J. E. Drake, *Inorg. Chem.* **30**, 3167 (1991).
18. Y. Garcia *et al.*, *Chem. Mater.* **10**, 2426 (1998).
19. O. Roubeau, J. G. Haasnoot, E. Codjovi, F. Varret, J. Reedijk, *Chem. Mater.* **14**, 2559 (2002).
20. T. Kitazawa *et al.*, *J. Mater. Chem.* **6**, 119 (1996).
21. V. Niel, J. M. Martinez-Agudo, M. C. Muñoz, A. B. Gaspar, J. A. Real, *Inorg. Chem.* **40**, 3838 (2001).
22. **1·(EtOH)**: $C_{46}Fe_2H_{38}N_{20}O_1S_4$, M = 1126.88, monoclinic, $C2/c$. For T = {150(2), 25(2)} K: a = {17.838(4), 17.803(6)}; b = {30.694(6), 30.608(10)}; c = {20.042(4), 19.843(6)} Å, β = {90.016(4), 90.124(5)}, V = {10973(4), 10813(6)} Å^3, Z = 8, μ(Mo-Kα) = {0.735, 0.746} mm^{-1}. Data were collected on two separate crystals on a Bruker Smart 1000 CCD equipped with Mo-K_α (λ = 0.71073 Å) radiation and Oxford Instruments nitrogen gas and helium gas cryostreams. Full-matrix least squares refinement on F_o^2 converged to $R1$ = {0.0582, 0.0924}, $wR2$ = {0.1118, 0.2179}. [See (*35*) for details.]
23. M. Kondo *et al.*, *Chem. Mater.* **12**, 1288 (2000).
24. **1**: $C_{22}Fe_1H_{16}N_{10}S_2$, M = 540.04, orthorhombic, *Ibam*, a = 8.418(19), b = 16.70(4), c = 20.62(5) Å, V = 2899(12) Å^3, T = 375(2) K, Z = 4, μ (Mo-Kα) = 0.692 mm^{-1}. Full matrix least-squares refinement on F_o^2 converged to $R1$ = 0.1143, $wR2$ = 0.2447. [See (*35*) for details.]
25. D. R. Corbin *et al.*, *J. Am. Chem. Soc.* **112**, 4821 (1990).
26. J. L. Atwood, J. E. D. Davies, D. D. MacNicol, F. Vögtle, Eds., *Comprehensive Supramolecular Chemistry* (Pergamon Press, New York, 1996), vol. 6.
27. O. Kahn, J. Larionova, J. V. Yakhmi, *Chem. Eur. J.* **5**, 3443 (1999).
28. C. J. Kepert, D. Hesek, P. D. Beer, M. J. Rosseinsky, *Angew. Chem. Int. Ed.* **37**, 3158 (1998).
29. C. J. Kepert, M. J. Rosseinsky, *Chem. Commun.* **1999**, 375 (1999).
30. H. Li, M. Eddaoudi, M. O'Keeffe, O. M. Yaghi, *Nature* **402**, 276 (1999).
31. K. Biradha, Y. Hongo, M. Fujita, *Angew. Chem. Int. Ed.* **39**, 3843 (2000).
32. B. F. Abrahams, P. A. Jackson, R. Robson, *Angew. Chem. Int. Ed.* **37**, 2656 (1998).
33. Powder x-ray diffraction measurements were made in situ during guest desorption and resorption under controlled environment (temperature and vapor) conditions. Refined unit cells for the resorbed phases at 303 K: **1·(EtOH)**, a = 18.041(3), b = 31.174(4), c = 19.908(6) Å, β = 90.28(3); **1·(MeOH)**, a = 17.987(3), b = 31.132(4), c = 19.851(6) Å, β = 89.98(3); **1·(PrOH)**, a = 18.12(2), b = 31.27(3), c = 19.85(4) Å, β = 89.8(2). [See (*35*) for details.]
34. The observed decrease in the Fe2-N bond lengths of ca. 0.07 Å is lower than the 0.1 to 0.2 Å expected for spin crossover in Fe(II) (*9*) and may reflect a degree of trapping of the high-spin state at the Fe2 site caused by the quench-cooling of the crystal to 25 K.
35. Single-crystal and powder XRD data, thermogravimetric analyses, magnetic data, Mössbauer data are available (see Materials and Methods, SOM Text, figs. S1 to S9, and tables S1 to S20). Crystallographic data were deposited in the Cambridge Crystallographic Database Centre [**1·(EtOH)** (150 K): CCDC-189340; **1·(EtOH)** (25 K): CCDC-189341; **1** (375 K): CCDC-189342].

36. Supported by the Australian Research Council (C.J.K. and K.S.M.).

Supporting Online Material

www.sciencemag.org/cgi/content/full/298/5599/1762/DC1
Materials and Methods
SOM Text
Figs. S1 to S9
Tables S1 to S20

10 July 2002; accepted 25 October 2002

Seismotectonics of Mid-Ocean Ridge Propagation in Hess Deep

Jacqueline S. Floyd,[1,2]* Maya Tolstoy,[2] John C. Mutter,[1,2,3] Christopher H. Scholz[1,2]

Hydroacoustic data from the eastern equatorial Pacific reveal low-magnitude seismicity concentrated at the propagating tip of the Galapagos Rise in Hess Deep. The patterns of seismicity and faulting are similar to those observed in the process zone of laboratory-scale propagating tensile cracks. Because the fracture energy required for propagation scales with crack length and process zone size, it follows that ridges can propagate stably in the brittle crust without exceptional resisting forces as proposed by previous models based on linear elastic fracture mechanics.

Lithospheric rifting and mid-ocean ridge propagation are the processes by which ocean basins are formed on Earth. Ridge propagation traditionally has been studied using the linear elastic fracture mechanics (LEFM) approach, in which the ridge is idealized as a tensile crack in an elastic plate and propagation occurs when the stress at the tip reaches a critical value (*1–3*). Few studies of ridge propagation have relied on earthquake data, because ridge earthquake magnitudes typically lie below the ~4.5 moment magnitude (M_w) detection threshold of teleseismic networks. Hydroacoustic monitoring in the eastern equatorial Pacific Ocean (*4*), however, has recently provided long-term records of low-magnitude (M_w ~ 1.8 to 4.4) seismicity at the propagating tip of the Galapagos Rise in Hess Deep (Fig. 1). We present observations of hydroacoustic seismicity and faulting in Hess Deep, which provide an opportunity to study the dynamics of ridge propagation and to test models based on the LEFM approach.

The Galapagos Rise is an intermediate-rate (4.5 to 6.0 cm/year full rate) spreading center that is propagating at ~6.5 cm/year (*5*) into oceanic crust 300,000 to 1 million years old accreted at the fast-spreading (13.5 cm/year full rate) East Pacific Rise (EPR). Regionally, the Galapagos Rise and EPR form a triple junction; however, multibeam bathymetry data show that the two ridges do not intersect (*6*) (Figs. 1 and 2). The Galapagos Rise volcanic ridge is identified as an elongate bathymetric high that reaches ~15 km into the 5.4-km-deep Hess Deep rift (Fig. 2). Hess Deep is bounded by two major normal faulted margins and contains a northward-

[1]Department of Earth and Environmental Sciences, [2]Lamont-Doherty Earth Observatory, [3]Earth Institute, Columbia University, 61 Route 9W, Palisades, NY 10964, USA.

*To whom correspondence should be addressed. E-mail: jsfloyd@ldeo.columbia.edu

strong background fluorescence. In contrast, injection of green fluorescent protein (GFP) as a tracer (e.g., by injection of RNA that encodes GFP) requires time for GFP to be expressed at levels detectable in vivo. (vi) Examination of the embryos at tadpole stages also showed that strong QD fluorescence was visible even in high-background regions such as the embryo gut (Fig. 3, H and I). (vii) The QD-micelles were much more resistant to photobleaching than were other fluorophores in vivo, which has been shown previously in vitro (*4*). Figure 4 compares the in vivo fluorescence quenching of QD-micelles and rhodamine green–dextran (RG-D). QD-micelles and RG-D were microinjected into sibling embryos that were at similar stages of development and had progressed to late blastula when they were imaged by time-lapse microscopy. After 80 min of constant illumination (at 450 nm) under the microscope, the QD fluorescence intensity remained unchanged (Movie S1), whereas the dextran had photobleached. Experiments with a membrane-bound GFP (EGFP fused to the Ras farnesylation sequence) gave similar results, with the QDs showing increased stability (fig. S1).

Although at early embryonic stages, QDs appeared to be diffusely localized throughout the cell, at later stages they concentrated in the cell nuclei (Fig. 3G). Time-lapse microscopy (Movies S2 and S3) revealed that this translocation to the nucleus occurs at a stage that phenotypically resembles the mid-blastula transition (MBT) (*28*), a critical stage in amphibian development when zygotic gene transcription is initiated. Because QD-micelles do not bind to DNA directly, it would be interesting to explore the mechanism of this translocation. If translocation proves to be concomitant with MBT, QDs will enable us to observe MBT in vivo with single-cell resolution.

These results indicate that micelle-encapsulated QDs fulfill the promise of fluorescent semiconductor nanocrystals for both in vitro and in vivo studies. Compared to other systems, they simultaneously provide efficient fluorescence, a great reduction in photobleaching, colloidal stability in a variety of bioenvironments, and low nonspecific adsorption.

References and Notes

1. A. P. Alivisatos, *Science* **271**, 933 (1996).
2. C. B. Murray, D. J. Norris, M. G. Bawendi, *J. Am. Chem. Soc.* **115**, 8706 (1993).
3. M. A. Hines, P. Guyot-Sionnest, *J. Phys. Chem.* **100**, 468 (1996).
4. M. Bruchez, M. Moronne, P. Gin, S. Weiss, A. P. Alivisatos, *Science* **281**, 2013 (1998).
5. W. C. W. Chan, S. Nie, *Science* **281**, 2016 (1998).
6. F. Mikulec, thesis, Massachusetts Institute of Technology (1999).
7. H. Mattoussi *et al.*, *J. Am. Chem. Soc.* **122**, 12142 (2000).
8. D. Gerion *et al.*, *J. Phys. Chem. B* **105**, 8861 (2001).
9. J. Aldana, Y. A. Wang, X. G. Peng, *J. Am. Chem. Soc.* **123**, 8844 (2001).
10. E. R. Goldman *et al.*, *Anal. Chem.* **74**, 841 (2002).
11. D. Gerion *et al.*, *J. Am. Chem. Soc.* **124**, 7070 (2002).
12. W. J. Parak *et al.*, *Adv. Mater.* **14**, 882 (2002).
13. M. Dahan *et al.*, *Opt. Lett.* **26**, 825 (2001).
14. S. Pathak, S. K. Choi, N. Arnheim, M. E. Thompson, *J. Am. Chem. Soc.* **123**, 4103 (2001).
15. J. O. Winter, T. Y. Liu, B. A. Korgel, C. E. Schmidt, *Adv. Mater.* **13**, 1673 (2001).
16. S. J. Rosenthal *et al.*, *J. Am. Chem. Soc.* **124**, 4586 (2002).
17. Materials and methods are available as supporting material on *Science* Online.
18. K. Hristova, D. Needham, *Macromolecules* **28**, 991 (1995).
19. S. Belsito, R. Bartucci, G. Montesano, D. Marsh, L. Sportelli, *Biophys. J.* **78**, 1420 (2000).
20. K. Kataoka, G. S. Kwon, M. Yokoyama, T. Okano, Y. Sakurai, *J. Control. Release* **24**, 119 (1993).
21. M. C. Jones, J. C. Leroux, *Eur. J. Pharm. Biopharm.* **48**, 101 (1999).
22. V. P. Torchilin, *Adv. Drug Delivery Rev.* **54**, 235 (2002).
23. M. Johnsson, P. Hansson, K. Edwards, *J. Phys. Chem. B* **105**, 8420 (2001).
24. C. G. Golander *et al.*, in *Poly(ethylene glycol) Chemistry*, J. M. Harris, Ed. (Plenum, New York, 1992), p. 221.
25. D. D. Lasic, M. C. Woodle, F. J. Martin, T. Valentincic, *Period. Biol.* **93**, 287 (1991).
26. C. A. Mirkin, R. L. Letsinger, R. C. Mucic, J. J. Storhoff, *Nature* **382**, 607 (1996).
27. A. P. Alivisatos *et al.*, *Nature* **382**, 609 (1996).
28. J. Newport, M. Kirschner, *Cell* **30**, 675 (1982).
29. C. A. Leatherdale, W.-K. Woo, F. V. Mikulec, M. G. Bawendi, *J. Phys. Chem.* **106**, 7619 (2002).

30. We thank H. Shio for assistance with electron microscopy and R. Harland (University of California, Berkeley) for membrane-GFP constructs. B.D. was supported in part by the Norman and Rosita Winston Fellowship. V.N. was supported in part by the Burroughs Wellcome Foundation. P.S. and A.H.B. are supported by funds from the Steinbach Fund and the Rockefeller University. B.D. acknowledges discussions with S. M. Simon and J. K. Jaiswal.

Supporting Online Material

www.sciencemag.org/cgi/content/full/298/5599/1759/DC1
Materials and Methods
Fig. S1
Movies S1 to S3

9 August 2002; accepted 28 October 2002

Guest-Dependent Spin Crossover in a Nanoporous Molecular Framework Material

Gregory J. Halder,[1] Cameron J. Kepert,[1]* Boujemaa Moubaraki,[2] Keith S. Murray,[2] John D. Cashion[3]

The nanoporous metal-organic framework $Fe_2(azpy)_4(NCS)_4$·(guest) (azpy is *trans*-4,4′-azopyridine) displays reversible uptake and release of guest molecules and contains electronic switching centers that are sensitive to the nature of the sorbed guests. The switching of this material arises from the presence of iron(II) spin crossover centers within the framework lattice, the sorbed phases undergoing "half-spin" crossovers, and the desorbed phase showing no switching property. The interpenetrated framework structure displays a considerable flexibility with guest uptake and release, causing substantial changes in the local geometry of the iron(II) centers. The generation of a host lattice that interacts with exchangeable guest species in a switchable fashion has implications for the generation of previously undeveloped advanced materials with applications in areas such as molecular sensing.

The self-organization of molecular species is fundamental to the generation of nanoscale molecular architectures that have specific structures and functions (*1*, *2*). In the area of porous metal-organic frameworks, the structural versatility of molecular chemistry has allowed the rational design and assembly of materials having novel topologies and exceptional host-guest properties (*3*–*8*). There has been comparatively little attention, however, on exploiting the many unique electronic aspects of molecular chemistry to impart specific electronic function to these materials. We report here on the incorporation of electronic switches, in the form of spin crossover centers, into porous molecular framework lattices.

Spin crossover centers are a well-known form of molecular switch in which a change in the electronic configuration at a metal center (high-spin ↔ low-spin) leads to distinctive changes in molecular geometry, color, and magnetism (*9*). The phenomenon may be stimulated by electromagnetic radiation or by variation of temperature and/or pressure. The generation of cooperative systems that display metastability and therefore hysteresis, including with light-induced excited spin state trapping (*10*), has drawn attention to the use of spin crossover centers in areas such as data storage and displays (*11*). An important approach for achieving cooperative interactions, both steric and magnetic, is the direct molecular linkage of metal sites in supramolecular (*12*, *13*) and framework (*14*–*21*) sys-

[1]School of Chemistry, University of Sydney, Sydney, NSW 2006, Australia. [2]School of Chemistry, Post Office Box 23, [3]School of Physics and Materials Engineering, Post Office Box 27, Monash University, Melbourne, VIC 3800, Australia.

*To whom correspondence should be addressed. E-mail: c.kepert@chem.usyd.edu.au

tems. We present a spin crossover material where the molecular linkages are of sufficient strength and arrangement to generate a porous framework that is robust to the uptake and removal of guest species, thereby providing a unique coexistence of nanoporosity and spin crossover in one material.

Monophasic dark red crystals of **1·(EtOH)**, $Fe_2(azpy)_4(NCS)_4$·(EtOH) (azpy is *trans*-4,4′-azopyridine and EtOH is ethanol), were synthesized by the slow diffusion of stoichiometric amounts of $Fe^{II}(NCS)_2$ and azpy in ethanol. The crystal structure of **1·(EtOH)** (*22*) consists of the double interpenetration of two-dimensional rhombic grids [i.e., (4, 4) networks] that are constructed by the linkage of Fe(II) centers by azpy units. The compressed octahedral coordination around the iron centers is completed by two axial thiocyanate ligands bound through the nitrogen donor. A full picture of the structure and a network representation showing the interpenetration of the grids are given in Figs. 1 and 2, respectively. The structurally equivalent rhombic grids interpenetrate in a manner similar to that seen previously in related metal-organic frameworks (*14*, *23*), generating 1-D channels parallel to the *c* axis. In the as-grown material, half of these channels are occupied by ethanol molecules to generate a "chessboard"–like pattern. This alternating distribution causes the framework to be distorted away from regular interpenetration so that the occupied and empty channels have dimensions of 10.6 × 4.8 Å and 7.0 × 2.1 Å and relative crystal volumes of 9 and 3%, respectively. The structure contains two crystallographically distinct Fe(II) centers with very similar ligand-binding geometries but different second coordination spheres; the ethanol OH groups form H-bonds with the sulfur atoms of the thiocyanate ligands bound to Fe2 but not with the thiocyanates bound to Fe1 (Fig. 3). The ethanol molecule is disordered over two orientations, and the relative distances of Fe1 and Fe2 to the disordered ethanol oxygen atom are 8.2 to 8.5 Å and 5.7 to 6.1 Å, respectively.

Complete and rapid desorption of the ethanol guests occurs with heating to 100°C, beyond which the empty framework material **1**, $Fe(azpy)_2(NCS)_2$, is stable to 140°C. To investigate the structural consequences of desorption, we heated a single crystal of **1·(EtOH)** in situ to 375 K under dry nitrogen on a single-crystal x-ray diffractometer and collected and analyzed a full data set for **1** (*24*). With ethanol removal, the general structural motif of interpenetrating grids remains intact, but the structure undergoes a number of changes (Fig. 1). Most notably, there is a scissors-like motion of the interpenetrating grids to decrease the angle of interpenetration, θ (defined in Fig. 2B), from 60.3° to 53.6°. This structural hinging causes an elongation and constriction of the 1-D channels, with their dimensions changing to 11.7 × 2.0 Å and the pore volume decreasing from 12 to 2%. On heating, the crystal volume increases by 6% and the macroscopic dimensions of the crystals change by −6, +9, and +3% along the *a*, *b*, and *c* axes, respectively, an effect that we were able to observe under the microscope. A slippage of the grids accompanies the hinging motion, with one set of parallel layers undergoing a translation of 1.0 Å along the *c* axis with respect to the other so that the iron atoms sit perfectly in the center of the rhomboids of the interpenetrated grids (Fig. 3). With the transition to regular interpenetration, the crystal symmetry increases from *C*-centered monoclinic (*C*2/*c*) to *I*-centered orthorhombic (*Ibam*) in a unit cell that is halved in both the *a* and *b* directions. This increase in symmetry causes the 1-D channels to become structurally equivalent and has the important consequence that the two distinct Fe(II) centers in **1·(EtOH)** merge to become a single, equivalent center in **1**. The relative geometries of both the azpy and thiocyanate units change appreciably with desorption; the thiocyanate units straighten and the pyridyl groups rotate so that their dihedral angles across the Fe(II) centers decrease from {69, 83}° and {−83, −73}° for Fe1 and Fe2, respectively, in **1·(EtOH)** to 0° for Fe1 in **1** (Fig. 3). This highly flexible property of a nanoporous molecular framework is reminiscent of the unusual behavior of zeolite RHO (*25*) and many clathrate-type systems (*26*–*28*) and is in contrast to other nanoporous molecular phases (*29*–*32*) and most classical porous solids where guest loss typically involves no change in symmetry and only minimal structural change.

Powder x-ray diffraction and thermogravimetry of **1·(EtOH)** performed with heating and cooling under controlled atmospheres indicated that guest desorption is a reversible process. On heating a polycrystalline sample of **1·(EtOH)** under a dry nitrogen atmosphere, we observed a large change in the diffraction pattern between 323 and 363 K, and the patterns for the fully sorbed and desorbed phases were consistent with the in situ single-crystal x-ray diffraction results. After cooling under an ethanol-vapor–nitrogen atmosphere, the sample reverted sharply back to the original pattern between 343 and

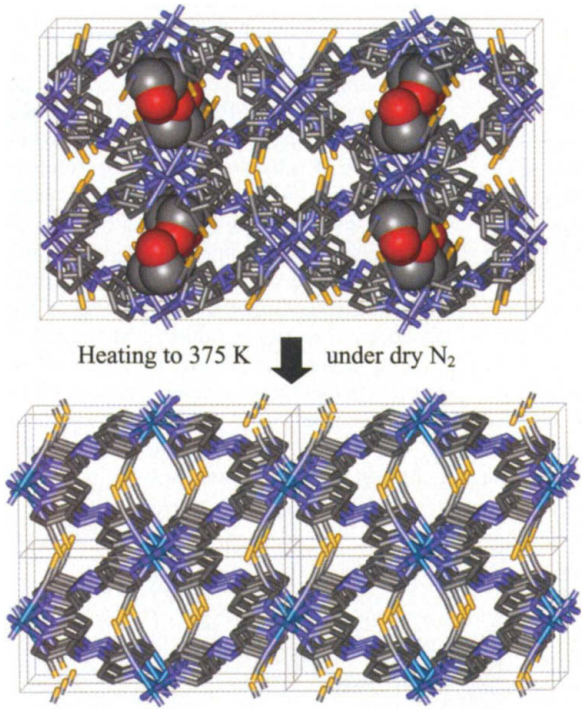

Fig. 1. X-ray crystal structures of **1·(EtOH)** at 150 K and **1** at 375 K, viewed approximately down the 1-D channels (*c* axis). Framework atoms are represented as sticks and atoms of the ethanol guests as spheres. In **1·(EtOH)** the ethanol guests occupy every second 1-D channel in a "chessboard" arrangement. Removal of ethanol by heating gives single crystals of **1**, which has empty, equivalent 1-D channels and a concomitant quartering of the unit cell. Hydrogen atoms are omitted for clarity.

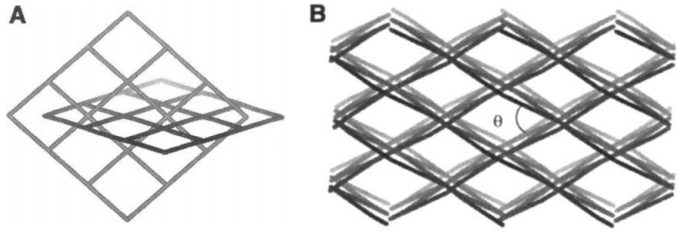

Fig. 2. A diagrammatic representation of the interpenetration of infinite $Fe(azpy)_2$ rhombic grids in **1·(EtOH)**, perpendicular to one of the grids (**A**) and approximately perpendicular to both (**B**), corresponding to the view given in Fig. 1. The layer interpenetration angle, θ, is defined in (B).

333 K (fig. S4). A thermogravimetric investigation indicated a circa (ca.) 80% sorption under similar conditions (fig. S1). The sorption of methanol and 1-propanol were also explored and gave patterns and unit cell analyses very similar to that of **1·(EtOH)** (figs. S3 and S5). The interpenetration angles (θ) for the sorbed phases derived directly from the unit cell dimensions (*33*) were 60.0°, 60.1°, and 60.2° for the methanol, ethanol, and 1-propanol adducts, respectively, indicating that the extent of opening of the hinged framework is subtly dependent on the size and shape of the sorbed guest molecules.

Magnetic susceptibility and Mössbauer effect spectral measurements were used to probe the spin states and spin changes in **1·(EtOH)** and in its desorbed and resorbed forms. In Fig. 4, the μ_{eff} (where μ_{eff} is the effective magnetic moment) values for **1·(EtOH)** remain essentially constant at 5.3 μ_B (where μ_B is the Bohr magneton) between 300 and 150 K, due to all Fe(II) sites being in the high-spin, $S = 2$, state. The Mössbauer spectrum at 295 K yielded only one quadrupole doublet with characteristic $S = 2$ values of the isomer shift $\delta = 0.97$ mm s^{-1} and the quadrupole splitting $\Delta E_Q = 2.57$ mm s^{-1}, even though there are two crystallographically distinct Fe sites. Below 150 K the magnetic moments decrease, rapidly at first (150 to 130 K) and then more gradually, reaching a constant value of 3.65 μ_B below 50 K. This value is indicative of only one of the two inequivalent Fe(II) sites being in the low-spin, S = 0, state after a 50% spin crossover. Mössbauer spectra taken at 6 K (fig. S6A) showed two quadrupole doublets due to coexisting high-spin ($\delta = 1.11$ mm s^{-1}, $\Delta E_Q = 2.97$ mm s^{-1}) and low-spin ($\delta = 0.45$ mm s^{-1}, $\Delta E_Q = 0.19$ mm s^{-1}) sites. There is little, if any, hysteresis in the μ_{eff} values as the temperature is slowly raised and lowered in the 50 to 150 K region. An absence of hysteresis is not uncommon for such systems (*12*, *14*, *15*), and we speculate that the flexibility of the material may facilitate a low-energy pathway between the high-spin and high/low-spin structures in this temperature range. A crystal structure determination at 25 K (*22*) suggests that it is Fe2, the iron center involved in H-bonding to the ethanol guest (Fig. 3), that undergoes spin crossover; the Fe2 average Fe-N(thiocyanate) and Fe-N(azpy) distances decreased by 0.06 and 0.07 Å, respectively, as compared to decreases of only 0.02 and 0.03 Å for Fe1 (*34*). An important consequence of the spin crossover is a contraction of the rhombic grids: The average Fe-Fe distance along the sides of the grids decreases from 13.38 to 13.30 Å with cooling from 150 to 25 K. The close similarity of coordination geometries of Fe1 and Fe2 above the crossover temperature indicates that the ethanol guest has only a very subtle influence on the geometry of the iron centers and suggests that the electronic influence of this molecule, through a H-bonding interaction with the thiocyanate group of Fe2, may play an important role in fine-tuning the ligand field splitting for spin crossover at this center.

When the ethanol guests are fully removed from the framework to give the desorbed phase, **1**, which has a substantially altered Fe(II) coordination geometry, the magnetic and Mössbauer data are compatible with the existence of high-spin Fe(II) sites only [$\mu_{eff} = 5.2$ μ_B at 300 K, 5.1 μ_B at 50 K, and 4.0 μ_B at 4 K (Fig. 4), isomer shift at 6 K of 1.14 mm s^{-1} and quadrupole splitting of 2.50 mm s^{-1} (fig. S6B)]. Zero-field splitting rather than spin crossover causes the downturn in the effective moment at low temperature. The absence of spin crossover is consistent with our view that the interaction of the H-bonded guest has an important electronic influence on the Fe(II) sites. Presumably of greater importance, however, is the absence of the steric influence of the guest, leading to considerable modifications of the framework and coordination geometries as described here.

The most notable magnetic data were obtained on sorption of other solvate molecules back into the channels of the desorbed network. The immersion of **1** in anhydrous methanol to give **1·(MeOH)** yielded magnetic moment data again indicative of spin crossover of half of the iron sites, with a μ_{eff}-versus-T plot that is similar to that of **1·(EtOH)** although without the sharp increase at ca. 140 K (see inset to Fig. 4). Exposure of this methanol solvate to the atmosphere at room temperature for periods of 4 to 12 hours caused a gradual disappearance of the crossover and replacement by S = 2 behavior for the desorbed material. The inset to Fig. 4 shows the effect of warming the sample to room temperature within the magnetometer [labeled **1·*x*(MeOH)**, where $0 \leq x \leq 1$ (x is the solvation fraction)] and the effect of exposing the sample to air for 12 hours to give **1**. Immersion of this desorbed sample in anhydrous 1-propanol yielded a material that showed a clear two-step crossover, with a sharp decrease from 5.0 μ_B that occurred between 140 and 130 K reaching a plateau of 4.65 μ_B between 130 and 110 K followed by a broader decrease to reach 3.8 μ_B at ~70 K, a value again indicative of a ~50% spin conversion (Fig. 4). Presumably the origin of the two-step crossover here relates to a subtle structural effect that produces a system with two pairs of structurally inequivalent iron centers, as could be induced by symmetry-lowering caused by an ordering of the guest molecules in the 1-D channels.

We show that it is possible to make nanoporous frameworks that display spin crossover effects that are influenced by the reversible exchange of sorbed guest molecules. The present $Fe_2(azpy)_4(NCS)_4$·x(guest) system retains the parent framework structure during guest desorption and resorption cycles, with

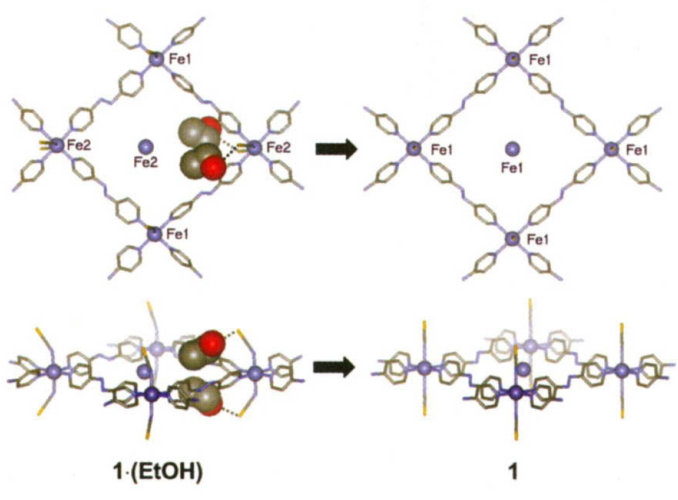

Fig. 3. The rhombic grid layers of **1·(EtOH)** and **1**. Removal of ethanol causes extensive modification to the structure, including a rotation of both the azpy and thiocyanate units, a translation of the interpenetrating layers by 1.0 Å (Fe atoms shown inside the rhomboids belong to the interpenetrating layers), and the removal of hydrogen-bonding interactions from the ethanol to the thiocyanate sulfur atoms (shown as dashed lines).

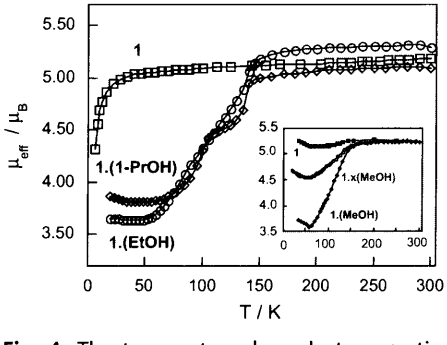

Fig. 4. The temperature-dependent magnetic moment of **1·x(guest)**, recorded on a single sample at different stages of guest desorption and resorption, showing 50% spin crossover behavior between 50 and 150 K for the fully loaded phases and an absence of spin crossover for the fully desorbed phase **1**. The ethanol- and methanol-loaded phases undergo a single-step spin crossover, whereas the 1-propanol adduct shows a two-step crossover with a plateau at 120 K. The inset shows the effect of partial and complete removal of methanol from **1·(MeOH)**.